Meteoritics & Planetary Science 40, Nr 8, 1159–1174 (2005)
Abstract available online at http://meteoritics.org

Defining the mechanisms that disturb the Sm-Nd isotopic systematics of the Martian meteorites: Examples from Dar al Gani 476 and Allan Hills 77005

J. EDMUNSON*, L. E. BORG, C. K. SHEARER, and J. J. PAPIKE

Institute of Meteoritics, University of New Mexico, Albuquerque, New Mexico 87131, USA
*Corresponding author. E-mail: edmunson@unm.edu

(Received 27 July 2004; revision accepted 29 June 2005)

Abstract–Microbeam studies of Martian meteorites Dar al Gani (DaG) 476 and Allan Hills (ALH) 77005 have been conducted to identify potential causes of disequilibrium exhibited in their Sm-Nd isotopic systematics. Olivine and maskelynite mineral fractions on the DaG 476 isochron are displaced relative to their positions as dictated by measured mineral compositions. The olivine mineral fractions from ALH 77005 not only have a relatively low Sm/Nd ratio, but appear to contain an unradiogenic component that shifts the olivine mineral fraction off the isochron defined by the pyroxene and maskelynite mineral fractions. Trace components such as melt inclusions, impact melt, high-Si mesostasis, and altered olivine were analyzed using scanning electron microscopy, quantitative electron microscopy, and secondary ion mass spectrometry to determine their potential for disturbing the isotopic systematics of the mineral fractions, assuming that the mineral fractions were not completely pure. Mixing models indicate that the presence of melt inclusions in the DaG 476 olivine mineral fraction lowered its Sm/Nd ratio. The maskelynite mineral fraction contains a related but more evolved mesostasis component that raised the Sm/Nd ratio of the fraction. The position of two olivine mineral fractions below the ALH 77005 isochron is interpreted to reflect small additions of impact melt with a light rare earth element enriched pattern and a non-indigenous, unradiogenic Nd component. Furthermore, the presence of rare earth elements in olivine and maskelynite from both igneous and non-igneous components such as melt inclusions, mesostasis, and impact melt is observed on a fine (<30 μm) scale. Despite the addition of this material, the Sm-Nd ages are not affected. This study demonstrates that detailed mineral separation procedures as employed by modern geochronology laboratories permit reliable ages to be derived from shocked and altered samples.

INTRODUCTION

Isotopic dating of Martian meteorites has proven to be difficult as a result of: 1) isotopic disequilibrium among igneous phases, 2) small sample sizes and low abundances of the elements of interest in many phases, 3) terrestrial alteration of meteorites that can both add and remove components from the bulk rock, and 4) redistribution and volatilization of elements during shock events (e.g., Nyquist et al. 1979; Shih et al. 1982; Jagoutz 1989; Borg et al. 2003). Traditionally, geochronologists have attempted to minimize these problems by assuming that mineral fractions that lie along a single line define a robust age, by leaching the samples in weak acids in order to remove terrestrial and Martian alteration products, and by applying multiple isotopic systems to single samples in order to determine concordant ages. Currently, the mechanisms responsible for the isotopic disturbances observed in the Martian meteorites are poorly understood. This study is designed to determine the mechanisms responsible for the Sm-Nd isotopic disequilibrium in mineral fractions from Dar al Gani (DaG) 476 and Allan Hills (ALH) 77005 using a microbeam analytical approach. This approach involves identifying contaminants that are present in the mineral fractions by using the scanning electron microscope, and quantifying their major element and rare earth element (REE) compositions by using the electron microprobe and the secondary ion mass spectrometer (SIMS). This information is used to define end-members of mixing models, which in turn constrain the components that are most likely to disturb the isotopic systematics of the olivine and maskelynite mineral fractions.

Samarium-neodymium dating of DaG 476 by Borg et al. (2003) yielded an age of 474 ± 11 Ma, based on an isochron that was defined by maskelynite, pyroxene, and olivine mineral fractions (Fig. 1a). Although the mineral fractions lie along a single line, making the isochron age robust, some of

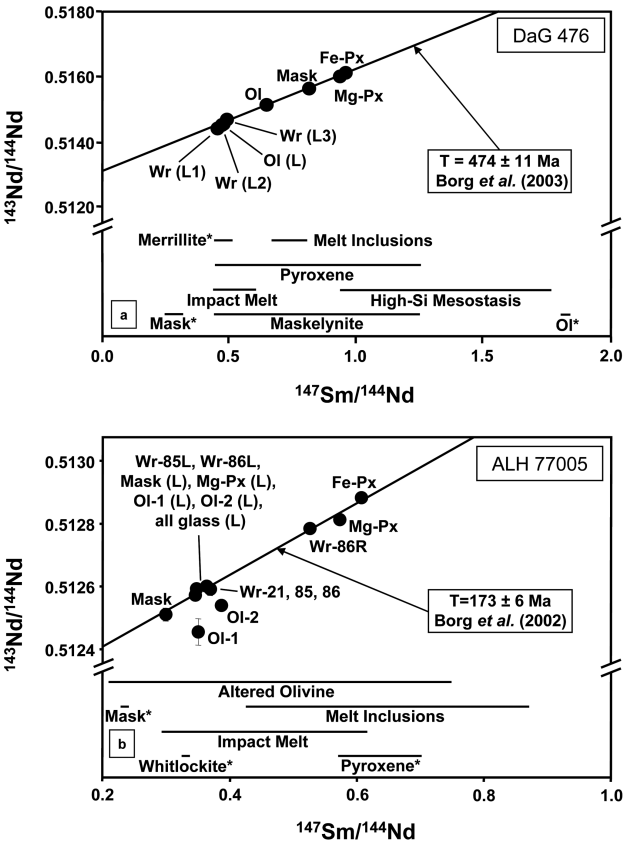

Fig. 1. Sm-Nd isochrons for DaG 476 and ALH 77005 after Borg et al. (2003) and Borg et al. (2002), respectively. All mineral fractions, except ALH 77005 whole rocks Wr-21, Wr-85, and Wr-86, were leached in HCl. Leachates are designated L. The lower portion of each diagram represents the range of $^{147}Sm/^{144}Nd$ ratios of materials determined during this study. a) Dar al Gani 476 isochron indicating an age of 474 ± 11 Ma. Note the relative positions of the olivine and maskelynite mineral fractions on the isochron. Also compare the $^{147}Sm/^{144}Nd$ ratios of the mineral fractions with those from Wadhwa et al. (2001) (denoted by *) at the bottom of the figure. Olivine $^{147}Sm/^{144}Nd$ ratios obtained during this study range from 0.33 to 1.66. b) Allan Hills 77005 isochron. Whole rocks, pyroxene, and maskelynite mineral fractions yield an age of 173 ± 6 Ma. The $^{147}Sm/^{144}Nd$ ratios of olivine from ALH 77005 in this study range from 0.30 to 0.84, and are not represented here. The mineral analyses denoted by * are from Lundberg et al. (1990).

the mineral fractions have $^{147}Sm/^{144}Nd$ ratios that are not indicative of chemical equilibrium among the phases. The DaG 476 maskelynite mineral fraction has a $^{147}Sm/^{144}Nd$ ratio of 0.81, whereas the olivine mineral fraction has a ratio of 0.65. These ratios contrast with the ion microprobe data obtained by Wadhwa et al. (2001) for the maskelynite and olivine minerals in thin section, which have $^{147}Sm/^{144}Nd$ ratios of 0.26 and 1.81, respectively. The difference in the $^{147}Sm/^{144}Nd$ ratios of the mineral fractions and the in situ mineral analyses suggests that the Sm/Nd ratios of the mineral fractions are either disturbed or not representative of the main mineral comprising the mineral fraction.

The Sm-Nd ages determined by Shih et al. (1982), Jagoutz (1989), and Borg et al. (2002) for the lherzolitic shergottite ALH 77005 are 325 ± 92 Ma, 135 ± 40 Ma, and 173 ± 6 Ma, respectively. The latter two ages are concordant and are similar to Rb-Sr ages obtained by Shih et al. (1982) and Borg et al. (2002), whereas the older Sm-Nd age of Shih et al. (1982) has been attributed to larger mass spectrometry uncertainties associated with their $^{143}Nd/^{144}Nd$ measurements (Borg et al. 2002). Although Borg et al. (2002) determined the most precise age for ALH 77005, the olivine mineral fractions have unexpectedly low $^{147}Sm/^{144}Nd$ ratios and lie below the isochron (Fig. 1b). The olivine mineral fractions of another lherzolitic shergottite petrologically similar to ALH 77005, Lewis Cliffs (LEW) 88516, show the same low $^{147}Sm/^{144}Nd$ ratios and also lie below the LEW 88516 Sm-Nd isochron (Borg et al. 2002). The fact that the olivine mineral fractions lie off the isochron suggests that the Sm-Nd isotopic compositions of the olivine mineral fractions are not in equilibrium with the maskelynite, pyroxene, and leachate fractions. The goal of this study is to determine the mechanisms responsible for the disturbances observed in the Sm-Nd isotopic systematics of DaG 476 and ALH 77005.

PETROLOGY OF DAR AL GANI 476 AND ALLAN HILLS 77005

Petrology of Dar al Gani 476

Dar al Gani 476 is a basaltic shergottite consisting of large olivines in a fine-grained groundmass of pyroxene and maskelynite (Zipfel et al. 2000). Goodrich (2002) classified DaG 476 and its paired samples (Dar al Gani 489, 670, 734, and 876) as olivine-phyric shergottites because of the porphyritic texture of the olivine, oxide composition, and modal augite abundance. The modal mineralogy ranges from 44–53% pigeonite, 12–17% maskelynite, 10–24% olivine, 3–13% augite, 4–7% impact melt, 2–4% orthopyroxene, 1–3% carbonates, 1–4% opaques (pyrrhotite, chromite, and ilmenite), and 1–2% merrillite (Mikouchi 1999; Zipfel et al. 2000; Folco et al. 2000; Wadhwa et al. 2001). The olivine contains small melt inclusions, which contain microlites of olivine, augite, and chromite, surrounded by a glass rich in Si and Al (Zipfel et al. 2000). Dar al Gani 476 has undergone terrestrial weathering, as evidenced by the alteration of silicate minerals, enrichment in La and Ce in olivines and pyroxenes, and the formation of secondary alteration products (Crozaz and Wadhwa 2001). Secondary alteration products in DaG 476 include carbonate veins, as well as trace amounts of gypsum, barite, and possibly phyllosilicates (Mikouchi 1999; Zipfel et al. 2000; Lee and Bland 2004). These products are likely of terrestrial origin because they are associated with fractures in the rock and have morphologies similar to those of known terrestrial weathering products (Mikouchi 1999). Furthermore, the calcite-rich leachates have $^{87}Sr/^{86}Sr$ ratios that match modern terrestrial seawater, Libyan soils, and impact melt glasses found in Libya (Borg et al. 2003).

Petrology of Allan Hills 77005

Allan Hills 77005 is a lherzolitic shergottite composed of cumulate olivines surrounded by poikilitic pyroxene and maskelynite (McSween et al. 1979; Lundberg et al. 1990). It contains approximately 60% olivine, 10% orthopyroxene, 10% maskelynite, 4% clinopyroxene, 3% oxides (chromite and ilmenite), with trace merrillite, pyrrhotite, and a FeO(OH) phase (McSween et al. 1979; Ikeda 1994; Treiman et al. 1994). Like DaG 476, ALH 77005 olivines contain melt inclusions. These inclusions contain maskelynite and microlites of pyroxene, as well as a high-Si phase that is interpreted to be coesite (Jagoutz 1989).

A noticeable feature of ALH 77005 is the brown coloration of olivine, attributed to the presence of approximately 4–5% Fe^{3+} in the olivine structure (Ostertag et al. 1984; Puga et al. 1998). Puga et al. (1998) argue that this brown coloration results from microexsolution of magnetite and enstatite. This texture is similar to that of terrestrial olivine symplectites, which contain microscopic dendrites of iron oxide and orthopyroxene. Oxidation of olivine during high temperature experiments has also produced symplectite structures (Haggerty and Baker 1967; Champness 1970; Putnis 1979). However, Bauer (1979) suggested that the homogeneous shock inclusion of an oxidizing atmosphere could also account for brown discoloration in olivine without microexsolution.

Xenocrystic Olivine in Dar al Gani 476 and Allan Hills 77005

Various workers have suggested that the olivines in both DaG 476 and ALH 77005 are xenocrystic, which could account for the disturbed nature of the olivine mineral fractions on the Sm-Nd isochrons. A xenocrystic origin for the olivine in DaG 476 is based on calculations that indicate a more magnesium-rich olivine would be the first phase to crystallize (Wadhwa et al. 2001). However, Zipfel et al. (2000) claim that a faster rate of diffusion in olivine during cooling may explain why the olivine phenocrysts in DaG 476 are in equilibrium with the groundmass clinopyroxene and not the Mg-rich orthopyroxene. Other evidence that supports a phenocrystic origin for the olivine is the fact that the olivine mineral fraction lies on the Sm-Nd isochron (Borg et al. 2003), indicating isotopic equilibrium between olivine, pyroxene, and maskelynite. Furthermore, the olivines have inclusions of chromite and pyroxene that are compositionally identical to those in the groundmass (Zipfel et al. 2000; Wadhwa et al. 2001). Thus, the disturbance of the Sm-Nd isotopic systematics of the DaG 476 olivine mineral faction is unlikely to reflect a xenocrystic origin of the olivine.

Olivines in ALH 77005 are argued to be xenocrystic because they are too Fe-rich to be in equilibrium with co-crystallizing Mg-rich pyroxenes (McSween et al. 1979; Lundberg et al. 1990). However, differences in the MgO/FeO ratios between olivine and pyroxene in ALH 77005 (and LEW 88516) have also been attributed to homogeneous re-equilibration of olivine with intercumulus liquid during cooling, which was not experienced by surrounding pyroxenes (Longhi and Pan 1989; Lundberg et al. 1990; Harvey et al. 1993). Zipfel and Goodrich (2001b) reconstructed the REE patterns of the parental melt for ALH 77005 from ion microprobe analyses of magmatic melt inclusions in olivine and found that they mirrored the REE pattern of the bulk rock as determined by Smith et al. (1984) and Warren et al. (1999). Finally, a phenocrystic origin for the olivines in both ALH 77005 and LEW 88516 is supported by the fact that the olivine mineral fractions lie on the Rb-Sr isochrons determined by Borg et al. (2002). These observations suggest that a xenocrystic origin is not responsible for the disturbances of the Sm-Nd isotopic systematics of the olivine mineral fractions in DaG 476 and ALH 77005.

ANALYTICAL METHODS

Unused mineral fraction grains from isotopic studies of Borg et al. (2002, 2003) and thin sections from DaG 476 and ALH 77005 were analyzed in this study. Mineral separation procedures for DaG 476 and ALH 77005 are described by Borg et al. (2003) and Borg et al. (2002), respectively. The unused mineral fraction grains were embedded in epoxy, polished, and carbon coated for analysis. Thin sections DaG 476 MPCh-5 from the Max-Plank Institut für Chemie, Mainz, Germany and ALH 77005 sections 30 and 34 from the NASA Johnson Space Center, Houston, Texas, USA were used for microbeam analysis.

Analytical work was conducted at the University of New Mexico on equipment operated by the Institute of Meteoritics. Scanning electron microscopy was completed using a JEOL JSM-5800LV SEM. Major element data was obtained using the JEOL Superprobe 733 electron microprobe (EMP) wavelength dispersive spectrometers operated at 15 kV with a beam current of 20 nA. Data were collected by an Oxford eXL II system and processed by a ZAF correction program. Glasses such as maskelynite, impact melt, melt inclusions, and high-Si mesostasis, were analyzed using a 10 μm beam to maximize sodium counts. Olivine and pyroxene were analyzed with a 1 μm beam. Counting times were 20 sec for major elements and 30 sec for minor elements. Secondary standards chosen for each unknown had compositions and structures similar to those of the unknown.

Trace elements were analyzed with a Cameca ims 4f secondary ion mass spectrometer. A 10 kV O^- primary beam with a current of 30 nA was applied to a spot approximately 30 μm in diameter. The sample voltage offset was −75 V with an energy window of ±25 V to minimize isobaric interferences. Analyses were completed with a 150 μm

secondary ion image field and a field aperture of 33 μm. Each spot was cleaned with a 125 μm raster for one to three minutes. Eight peak-hopping cycles were standard for each analysis. Isotopes analyzed included ^{30}Si, ^{139}La, ^{140}Ce, ^{146}Nd, ^{147}Sm, ^{151}Eu, ^{153}Eu, ^{163}Dy, ^{167}Er, ^{168}Er, and ^{174}Yb. Counting times varied based on the expected abundances of each isotope in each unknown. Olivine and pyroxene REE data were obtained using pyroxene standards Kh1 and Kaug. Maskelynite analyses were calibrated using plagioclase from the Moore County meteorite. Impact melt, melt inclusions, and high-Si mesostasis standards were rhyolitic glasses DM0, ATHO, and Macusami, and basaltic glasses Dr1-P3-4 and All93-11-103. The standards chosen for each glass calibration reflected the SiO_2 content of the unknowns. Absolute abundances of each element were calculated using natural isotopic abundances and trace element to ^{30}Si intensity ratios, normalized to the SiO_2 abundance of the unknown determined by EMP. Analytical uncertainties were calculated as standard error and are comparable to those of Lundberg et al. (1990) and Wadhwa et al. (2001). Spots chosen for SIMS analysis were based on the following criteria: 1) stoichiometry of the mineral and homogeneity of glasses determined by EMP, 2) sufficient size for analysis, and 3) sufficient distance from cracks and terrestrial alteration. Natural isotopic abundances of ^{147}Sm (0.1499) and ^{144}Nd (0.2380) were assumed in order to compare SIMS and thermal ionization mass spectrometer (TIMS) data. Chondritic REE abundances for text and figures were obtained from Anders and Grevesse (1989).

RESULTS

Numerous igneous phases, secondary alteration products, and impact melt glasses were analyzed in order to determine if a mechanical mixture of these components in the olivine and maskelynite mineral fractions from DaG 476 and ALH 77005 could account for the observed disturbances in the Sm-Nd isotopic systematics of the mineral fractions. The igneous minerals chosen for analysis appeared to be minimally altered by impact and terrestrial alteration processes. Melt inclusion analyses were completed on glasses and therefore reflect only those portions of the inclusions with the highest REE abundances. Consequently, these analyses cannot be used to calculate parental melt compositions. Potential impurities in the DaG 476 and ALH 77005 mineral separates include melt inclusions, impact melt, high-Si mesostasis, and alteration products. Descriptions of the mineral phases and potential impurities in the mineral fractions follow.

Composition of Minerals and Potential Contaminants in Dar al Gani 476

The olivines analyzed from DaG 476 in this study range in composition from Fo_{76} to Fo_{61} and are comparable in major element composition to those analyzed by both Zipfel et al. (2000) and Wadhwa et al. (2001) (Table 1). The olivine mineral data presented here have a less light rare earth element (LREE) depleted pattern and higher overall REE abundances (Nd abundances between 0.04 and 0.11 ppm) than those reported by Wadhwa et al. (2001) (Fig. 2). These olivines also do not show the enrichment in La and Ce observed by Wadhwa et al. (2001). The ^{147}Sm/^{144}Nd ratios and REE abundances obtained for the olivines during this study encompass the values determined for the olivine mineral fraction by Borg et al. (2003) (Table 2).

Maskelynites analyzed in DaG 476 range in composition between An_{67} and An_{52}, also comparable to analyses by Zipfel et al. (2000) and Wadhwa et al. (2001). The data obtained in this study indicate that the maskelynite has less LREE enrichment, elevated ^{147}Sm/^{144}Nd ratios, and higher overall REE abundances compared to those reported by Wadhwa et al. (2001). Nevertheless, the ^{147}Sm/^{144}Nd ratios and REE abundances measured here are similar to those of the maskelynite mineral fraction analyzed by Borg et al. (2003) (Table 2).

Small melt inclusions (5–50 μm) were observed in the DaG 476 olivines. These inclusions are completely enclosed by the host mineral and commonly appear as circular features with radiating fractures independent of linear $CaCO_3$-filled fractures (Fig. 3a). Many of these inclusions contain microlites of olivine and pyroxene surrounded by glass. Microprobe analyses of the glass in 11 magmatic inclusions yield SiO_2 ranges of 67–79 wt%, with a large range in P_2O_5 from 0.01 to 1.1 wt% (Table 1). The inclusions have a notable range in REE abundances (e.g., Nd ranges from 1 to 3 ppm), which correlate positively with P_2O_5. Like the melt inclusions in Sayh al Uhaymir 005 (Zipfel and Goodrich 2001a), the melt inclusion glasses in DaG 476 have LREE-depleted patterns that mimic the bulk rock pattern determined by Barrat et al. (2001). However, unlike the bulk rock, they exhibit negative Eu anomalies indicative of plagioclase fractionation (Fig. 2, Table 1).

Impact melt glass is also present in DaG 476 as veins or small isolated pockets (Fig. 3b). This glass has SiO_2 abundances ranging from 30–53 wt% and P_2O_5 abundances ranging from 0.01–1.3 wt% (Table 1). The REE abundances measured in the impact melt vary greatly (Fig. 2). Neodymium, for example, ranges from 0.2 to 1.6 ppm. The large range in P_2O_5 may be indicative of inclusion of various amounts of a merrillite component into the melt during shock, which could account for the range of REE abundances observed in the impact melt. This is supported by the direct correlation between P_2O_5 and Nd abundances, as well as the shape of the impact melt REE patterns which are similar to DaG 476 phosphates (Wadhwa et al. 2001).

A high-Si mesostasis was identified in maskelynite and pyroxene mineral fraction grains. This amorphous material appears to fill interstices between minerals (Fig. 3c). Analyses of the high-Si mesostasis indicate that the SiO_2

Table 1. Representative analyses of minerals and glasses in DaG 476.

	Olivine		Pyroxene		Maskelynite		Magmatic melt inclusions			Impact melt		High-Si mesostasis	
Point	Ol1d	Ol2c	Px3b	Px4a	M2b	T1m5	G13[a]	G14	G17	Imp3e	T2g9	G1um	G410
SiO_2	38.1	36.0	51.4	53.6	51.9	52.8	71.4	75.9	70.8	46.1	53.5	89.8	82.1
TiO_2	n.d.	0.02	0.48	0.15		0.14	0.31	0.40	0.37	1.67	0.17	0.08	0.07
Al_2O3	0.06	n.d.	1.67	1.00	31.0	27.5	18.0	16.1	18.0	2.32	1.10	0.54	0.90
Cr_2O_3	0.05	0.04	0.81	0.61		0.13				2.08	0.53		
FeO	21.4	33.2	11.3	15.7	0.41	2.06	1.95	0.84	1.48	17.9	15.8	1.12	0.89
MnO	0.46	0.72	0.47	0.60		0.10				0.56	0.62		
MgO	39.1	29.7	16.0	23.7		2.08	0.50	0.25	0.21	18.8	23.1	0.02	0.05
CaO	0.16	0.23	15.9	4.27	13.0	10.9	5.22	5.94	2.30	7.22	4.59	0.07	0.08
Na_2O	n.d.	n.d.	0.18	0.06	3.75	4.03	2.19	1.12	1.06	0.32	0.04	n.d.	0.01
K_2O					0.05	0.06	0.67	0.32	1.03	n.d.	n.d.	0.04	0.02
P_2O_5						0.16	0.94	0.25	0.73	1.26	0.03	n.d.	n.d.
SO_3						n.d.	0.04	0.04	0.02	0.02	n.d.	0.06	0.10
Total	99.3	99.9	98.2	99.7	100.1	100.0	101.2	101.1	96.0	98.3	99.5	91.7	84.2
	Fo_{76}	Fo_{65}	En_{43} Wo_{35}	En_{61} Wo_9	An_{66}	An_{60}							
La		0.00 ± 0.01	0.01 ± 0.01	0.01 ± 0.01	0.03 ± 0.01	0.06 ± 0.01	0.37 ± 0.03	0.25 ± 0.02	0.54 ± 0.03	0.25 ± 0.01	0.04 ± 0.01	0.03 ± 0.01	0.01 ± 0.01
Ce	0.01 ± 0.01	0.02 ± 0.01	0.03 ± 0.01	0.03 ± 0.01	0.06 ± 0.01	0.08 ± 0.01	0.63 ± 0.03	0.69 ± 0.03	1.78 ± 0.14	1.29 ± 0.01	0.15 ± 0.01	0.05 ± 0.01	0.12 ± 0.05
Nd	0.04 ± 0.01	0.03 ± 0.01	0.06 ± 0.01	0.09 ±0.01	0.10 ± 0.01	0.10 ± 0.01	1.32 ± 0.03	1.48 ± 0.01	2.64 ± 0.04	1.63 ± 0.02	0.21 ± 0.01	0.04 ± 0.01	0.15 ± 0.01
Sm	0.05 ± 0.01	0.08 ± 0.01	0.12 ± 0.01	0.12 ±0.01	0.09 ± 0.01	0.08 ± 0.01	1.44 ± 0.02	1.91 ± 0.01	2.78 ± 0.01	1.29 ± 0.01	0.16 ± 0.01	0.12 ± 0.01	0.23 ± 0.01
Eu	0.01 ± 0.01	0.01 ± 0.01	0.05 ± 0.01	0.04 ± 0.01	0.69 ± 0.01	0.91 ± 0.01	0.33 ± 0.01	0.21 ± 0.01	0.36 ± 0.02	0.44 ± 0.01	0.07 ± 0.01	0.01 ± 0.01	0.02 ± 0.01
Dy	0.09 ± 0.01	0.10 ± 0.01	0.36 ± 0.01	0.45 ±0.03	0.10 ± 0.01	0.32 ± 0.02	7.69 ± 0.22	5.23 ± 0.11	7.93 ± 0.16	6.31 ± 0.04	1.11 ± 0.06	0.23 ± 0.01	0.76 ± 0.02
Er	0.04 ± 0.01	0.07 ± 0.01	0.28 ± 0.02	0.53 ±0.04	0.05 ± 0.01	0.44 ± 0.02	3.83 ± 0.09	3.13 ± 0.05	3.49 ± 0.08	4.34 ± 0.05	1.09 ± 0.04	0.17 ± 0.01	0.62 ± 0.03
Yb	0.05 ± 0.01	0.06 ± 0.01	0.29 ± 0.01	0.22 ±0.01	0.03 ± 0.01	0.19 ± 0.01	3.73 ± 0.10	1.84 ± 0.05	3.83 ± 0.09	3.39 ± 0.05	0.66 ± 0.01	0.24 ± 0.01	0.54 ± 0.01
$^{147}Sm/^{144}Nd$	0.69 ± 0.04	1.66 ± 0.10	1.26 ± 0.16	0.82 ± 0.08	0.58 ± 0.02	0.48 ± 0.06	0.66 ± 0.02	0.78 ± 0.01	0.63 ± 0.01	0.48 ± 0.01	0.46 ± 0.05	1.78 ± 0.14	0.94 ± 0.04

[a]Average of two analyses.

Major element oxides in wt%. Trace element concentration in ppm. Error reported as standard error.

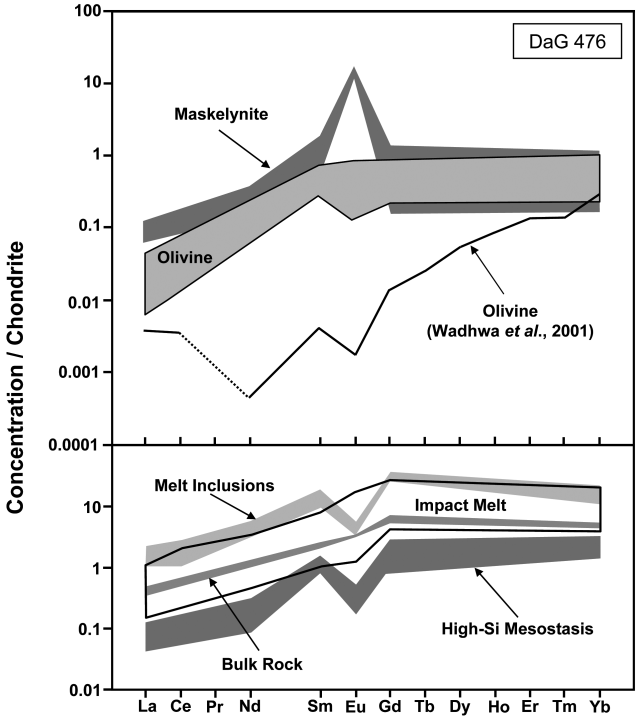

Fig. 2. Rare earth element patterns for DaG 476 olivine, maskelynite, melt inclusions, impact melt, and high-Si mesostasis from this study; the bulk rock determined by Barrat et al. (2001). Note that the melt inclusions, impact melt, and the high-Si mesostasis patterns are similar to the bulk rock pattern, except for the negative Eu anomalies. Also note the slight LREE depletion and larger negative Eu anomaly of the high-Si mesostasis compared to the melt inclusions. The Gd content of the Wadhwa et al. (2001) olivine was estimated from Sm and Tb contents. Praseodymium was below detection limits in the Wadhwa et al. (2001) pattern and was omitted during the creation of this pattern (dashed line).

abundances range from 75–90 wt% with minor amounts of Al_2O_3, FeO, MgO, and CaO (Table 1). This material yields low (84–92%) microprobe totals. Concurrent analysis of secondary standards and other phases on the grain mounts yielded satisfactory microprobe totals, suggesting that the high-Si mesostasis contains an element or elements that were not analyzed. Carbon dioxide solubility in high-Si melts is insufficient to account for the low microprobe totals (e.g., Mysen et al. 1976; Boettcher 1984; Pan et al. 1991). However, the low microprobe totals could be explained by hydration of this material. When compared to the melt inclusions, the high-Si mesostasis has REE abundances that are approximately 10 times lower (Fig. 2, Table 1). The REE patterns of the high-Si mesostasis are very similar to those of the melt inclusions, but are slightly more LREE-depleted and have slightly larger negative Eu anomalies (Fig. 2). Another high-Si material, determined to be altered impact melt, was observed in DaG 476 by Crozaz and Wadhwa (2001). It is characterized by high levels of Al, Ca, Mg, K, P, Ba, and Sr, accompanied by relatively extreme LREE enrichment and high abundances of REEs that are not observed in the high-Si mesostasis discussed here. Therefore, the high-Si mesostasis analyzed here is fundamentally different from the altered impact melt observed by Crozaz and Wadhwa (2001).

Composition of Minerals and Potential Contaminants in Allan Hills 77005

Analyses of olivines from ALH 77005 indicate that the olivines have a slightly larger range in forsterite content (Fo_{75}–Fo_{68}) than reported by Treiman et al. (1994) (Table 3). Although the olivine analyses are stoichiometric, a few olivines contain unusually high abundances of Al_2O_3, Cr_2O_3, and P_2O_5 for ALH 77005 olivines, in excess of 0.2 wt% (Table 3). Despite the presence of these additional elements, the olivine appears crystalline and unaltered. These analyses are not likely to be in error because the secondary standard analyses were satisfactory and because analyses were completed on spots that were isolated from impurities such as chromite, feldspar, merrillite, and melt inclusions. Although the majority of the olivine analyses in this study have higher REE abundances than those of Lundberg et al. (1990) (e.g., Nd abundances between 0.02 and 0.45 ppm), the REE patterns observed here for the olivines are typically more LREE-depleted (i.e., have a higher $^{147}Sm/^{144}Nd$ ratio) (Fig. 4, Table 3). For example, the $^{147}Sm/^{144}Nd$ ratios calculated for the Lundberg et al. (1990) olivine range from 0.20 to 0.30, whereas the $^{147}Sm/^{144}Nd$ ratios calculated during this study range from 0.30 to 0.84. The $^{147}Sm/^{144}Nd$ ratios calculated for the olivines from this study are comparable to the ratios of the olivine mineral fractions obtained by Borg et al. (2002) (Table 2). The wide range in $^{147}Sm/^{144}Nd$ ratios observed in the olivine, the presence of Fe^{3+} (e.g., Ostertag et al. 1984), and, in some cases, higher abundances of Al_2O_3, Cr_2O_3, and P_2O_5, suggest that the olivines in ALH 77005 have been significantly disturbed by a post-crystallization process.

An altered form of olivine observed in thin section 34 was also analyzed. It appears as mottled areas in olivines and is commonly associated with sulfur-rich veins (Fig. 5a), suggesting that it may be an alteration product. Therefore, this material is taken to be representative of the compositional effects of alteration on the olivines. The bulk of the altered olivine is composed of SiO_2 (40–67 wt%), FeO (12–24 wt%), and SO_3 (2–11 wt%) (Table 3). Low microprobe totals (83–94%) and the presence of FeO(OH) (McSween et al. 1979) suggest that the altered olivine is hydrated. Despite alteration, SIMS analyses of olivine surfaces with large portions of altered olivine yield REE patterns and abundances that are very similar to those obtained on unaltered olivine (Fig. 4, Table 3).

Melt inclusions were observed in olivines from both thin sections of ALH 77005 (Fig. 5b). Analyses of the glass portions of these inclusions have microprobe totals near 100%, indicating that they are not significantly hydrated. The glasses exhibit a wide range in SiO_2 abundances from 56–73 wt% (Table 3). When compared to melt inclusions in ALH

Table 2. Comparison of TIMS and SIMS data.

Fraction	Source	Sm (ppm)	Range in Sm (ppm)	Nd (ppm)	Range in Nd (ppm)	$^{147}Sm/^{144}Nd$	Range in $^{147}Sm/^{144}Nd$
DaG 476 phases							
Impact melt	This study	0.28	0.18–1.00	0.55	0.21–1.62	0.46	0.43–0.59
Mask R	Borg et al. (2003)	0.0587		0.0435		0.81489 ± 0.00163	
Maskelynite	This study	0.09	0.07–0.26	0.08	0.06–0.17	0.63	0.43–1.25
Fe-Px R	Borg et al. (2003)	0.0683		0.0417		0.96017 ± 0.00096	
Mg-Px R	Borg et al. (2003)	0.0697		0.0449		0.93813 ± 0.00103	
Pyroxene	This study	0.08	0.06–0.42	0.03	0.01–0.31	0.64	0.48–1.26
Ol R	Borg et al. (2003)	0.0759		0.0709		0.64795 ± 0.00065	
Olivine	This study	0.07	0.04–0.11	0.06	0.03–0.11	0.53	0.33–1.66
Melt inclusions	This study	2.08	1.44–2.78	1.57	1.32–2.64	0.70	0.63–0.78
High-Si mesostasis	This study	0.17	0.12–0.23	0.05	0.04–0.15	0.95	0.94–1.78
ALH 77005 phases							
Unleached Wr	Borg et al. (2002)	0.502		0.858		0.3580 ± 0.0004	
Wr-86 R	Borg et al. (2002)	0.092		0.107		0.5233 ± 0.0006	
Impact melt	This study	1.11	0.21–13.53	0.96	0.15–26.40	0.31	0.29–0.86
Mask R	Borg et al. (2002)	0.081		0.165		0.2969 ± 0.0003	
Px R[a]	Borg et al. (2002)	0.139		0.144		0.5879 ± 0.0007	
Ol R[a]	Borg et al. (2002)	0.010		0.017		0.3655 ± 0.0011	
Olivine	This study	0.12	0.03–0.22	0.12	0.02–0.45	0.55	0.30–0.84
Altered olivine	This study	0.08	0.02–0.18	0.03	0.01–0.41	0.26	0.21–0.75
Melt inclusions	This study	0.31	0.11–1.41	0.16	0.09–2.00	0.50	0.42–0.87

[a]Average of two analyses.

Concentration data are weighted averages of all analyses obtained during this study. Ranges indicate variations in concentrations and $^{147}Sm/^{144}Nd$ ratios observed throughout the study. Individual SIMS analyses have errors between 2 and 13%.

77005 olivine analyzed by Jagoutz (1989), the inclusions analyzed here have a wider range of FeO and MgO abundances, higher concentrations of Na_2O and K_2O, and a lower concentration of CaO. The REE patterns of the inclusions are roughly parallel to a melt inclusion analyzed by Zipfel and Goodrich (2001b), which was interpreted to represent the bulk melt inclusion composition, although the melt inclusions analyzed here have lower overall REE abundances (Fig. 4, Table 3).

Veins and pockets of impact melts were also observed throughout the ALH 77005 thin sections, commonly associated with olivine (Fig. 5c). They have a large range of SiO_2 content (35–71 wt%) and vary from 0–8 wt% P_2O_5 (Table 3). The REE abundances of the impact melt also have a wide range (e.g., Nd = 0.1 to 26 ppm) (Fig. 4). Like impact melt from DaG 476, the considerable range of P_2O_5 and REE abundances in the ALH 77005 impact melt suggests that it contains a variable contribution of merrillite (e.g., Fig. 5c).

DISCUSSION

Mixing models were created to illustrate the effects of adding specific contaminants (e.g., melt inclusions, impact melt, high-Si mesostasis, and alteration products) to "pure" mineral phases (e.g., olivine and maskelynite). In order to better constrain the effects on the Sm-Nd isochrons, Sm and Nd ratios and abundances are used in the models. The following is a summary of the results of mixing models generated with data obtained in this study as well as previously published mineral and mineral fraction data.

Mixing Models for Dar al Gani 476 Olivine and Maskelynite Compositions

The DaG 476 olivine and maskelynite mineral fractions do not lie along the isochron in positions that match estimates of the $^{147}Sm/^{144}Nd$ ratio of the olivine and maskelynite from Wadhwa et al. (2001) (Fig. 1a). There are two potential impurities that, if included in the olivine mineral fractions, could sufficiently affect the isotopic systematics: melt inclusions and impact melt (Figs. 1a and 3). The high-Si mesostasis was not used as an end-member in the models because this material did not have high enough REE abundances and low enough $^{147}Sm/^{144}Nd$ ratios to influence the composition of the olivine mineral fraction. Mixing models were generated using melt inclusions and impact melt as end-members, as well as the mineral data from Wadhwa et al. (2001), in an attempt to reproduce the Nd abundances and $^{147}Sm/^{144}Nd$ ratios of the olivine and maskelynite mineral fractions. The olivine analysis of Wadhwa et al. (2001) was used to define the "pure" olivine end-member because this composition has the lowest measured REE abundances and is therefore the best reflection of the igneous composition.

The mixing models demonstrate that 3% of the melt inclusion glass is needed to reproduce the composition of the

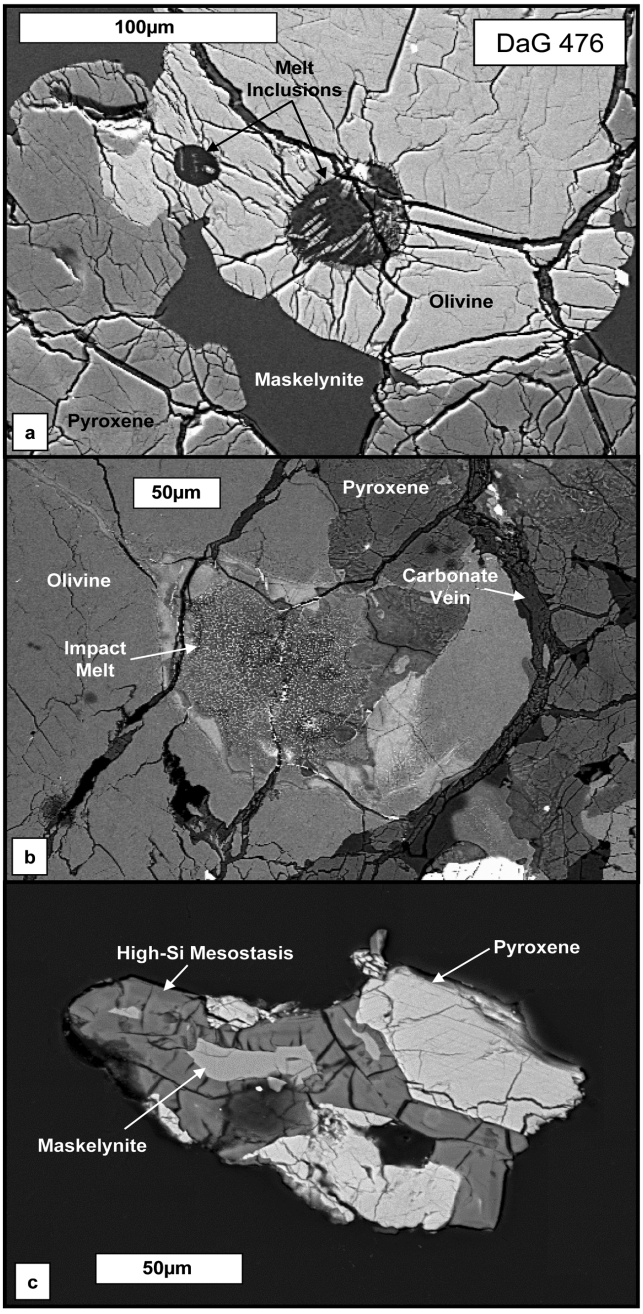

Fig. 3. SEM backscatter images of components in DaG 476. a) Two circular glassy melt inclusions in olivine. Note the characteristic radial fractures. Also note the dark areas within the glass; these portions are high in silica. b) Olivine and associated impact melt. c) Maskelynite mineral fraction grain. Note the presence of the high-Si mesostasis.

olivine mineral fraction, whereas roughly 4% of the impact melt is needed (Fig. 6). Although the models indicate that both melt inclusions and impact melt are equally viable contaminants, the impact melt is more likely to contain components that are not in isotopic equilibrium with the olivine, pyroxene, and maskelynite in DaG 476 (Rao et al. 1999). In order to maintain isotopic equilibrium between the olivine mineral fraction and other igneous phases, the impact melt must be derived from components within the rock. The observed presence of igneous melt inclusions in the olivines, combined with the fact that the olivine mineral fraction lies on the Sm-Nd isochron, suggests that the Sm-Nd isotopic disturbance of the olivine mineral fraction is the result of the incorporation of igneous melt inclusions. Note, however, that the addition of either the melt inclusions or an appropriate impact melt composition could account for the relatively low $^{147}Sm/^{144}Nd$ ratios and high REE abundances of the olivine mineral fraction compared to the olivine of Wadhwa et al. (2001).

The mixing of olivine and melt inclusions also reproduces the REE abundances (and patterns) of olivines analyzed in this study (Fig. 7). The olivine end-members of this model include a measured olivine composition (Wadhwa et al. 2001) and an average olivine composition in equilibrium with the bulk rock calculated by multiplying the bulk rock REE abundances of Barrat et al. (2001) and the partition coefficients in Table 4 (McKenzie and O'Nions 1991). The partition coefficients used in calculating the olivine composition reflect a fairly low $^{147}Sm/^{144}Nd$ ratio for olivine in equilibrium with the bulk rock, relative to other known partition coefficient sets (e.g., $D_{Sm}/D_{Nd} = 6$) (Snyder et al. 1992). Thus, the calculated olivine and the Wadhwa et al. (2001) olivine REE patterns reflect, with specific regards to the Sm/Nd ratio, the range of the most viable compositions for olivine in DaG 476. Note that the olivine composition from Wadhwa et al. (2001) has elevated La and Ce abundances and has therefore been significantly affected by terrestrial alteration (Wadhwa et al. 2001; Crozaz and Wadhwa 2001; Crozaz et al. 2003). Our modeling demonstrates, however, that the La and Ce added to the olivine by terrestrial alteration represents a trivial proportion of the total REEs in many olivine analyses and in the olivine mineral fractions (Fig. 7). Therefore, although the DaG 476 olivines are clearly altered, many appear to also contain a component derived from the melt inclusions. In fact, it is the melt inclusions that appear to dominate the REE budget and Sm-Nd isotopic systematics of these olivines.

Mixing models, generated using the maskelynite composition from Wadhwa et al. (2001) as one end-member, and either the melt inclusions or the high-Si mesostasis as the other end-member, are presented in Fig. 8. The impact melt was not included in this mixing model because it has a $^{147}Sm/^{144}Nd$ ratio that is not high enough to account for the $^{147}Sm/^{144}Nd$ ratio of the maskelynite mineral fraction on the isochron (Fig. 1a). Furthermore, Fig. 8 indicates that the melt inclusion glasses do not have high enough $^{147}Sm/^{144}Nd$ ratios to account for the high $^{147}Sm/^{144}Nd$ ratio of the maskelynite mineral fraction. Approximately 20% of the high-Si mesostasis is needed to reproduce the $^{147}Sm/^{144}Nd$ ratio of the maskelynite mineral fraction. However, 20% contamination

Table 3. Representative analyses of minerals and glasses in ALH 77005.

	Olivine			Altered olivine		Magmatic melt inclusions			Impact melt	
Point	30im1k	342ol3	34ox21	34ox4	341fe4	34ol2d	30oli1b	30im4b	30im5b	30im5c
SiO_2	37.5	37.1	37.6	67.1	57.9	56.3	68.6	42.8	36.3	31.7
TiO_2	0.05	0.05	n.d.	0.04	0.03	0.66	0.42	0.56	0.19	0.79
Al_2O_3	0.67	0.01	0.02	0.12	0.10	10.8	18.3	9.04	0.40	1.35
Cr_2O_3	0.63	0.03	0.05	0.15	0.08	0.02	n.d.	0.80	0.16	1.31
FeO	22.1	27.0	24.2	14.9	23.5	10.7	0.60	18.8	25.8	23.2
MnO	0.48	0.54	0.58	0.06	0.01	0.25	n.d.	0.44	0.63	0.52
MgO	37.7	35.2	37.1	0.74	0.61	13.1	0.19	20.9	34.1	29.0
CaO	0.54	0.23	0.24	0.04	0.02	4.59	1.78	4.30	1.46	6.17
Na_2O	0.04	n.d.	n.d.	0.19	0.04	2.47	6.76	1.78	0.04	0.16
K_2O	n.d.	n.d.	n.d.	0.69	0.42	0.60	1.97	n.d.	n.d.	n.d.
P_2O_5	0.14	n.d.	0.06	0.08	0.02	0.17	0.36	0.63	1.20	5.96
SO_3	n.d.	n.d.	0.01	2.48	1.98	0.04	0.02	0.04	n.d.	n.d.
Total	99.9	100.2	99.8	86.6	84.7	99.7	99.0	100.2	100.3	100.0
	Fo_{75}	Fo_{70}	Fo_{73}							
La	0.05 ± 0.01	0.56 ± 0.02	0.01 ± 0.01	0.22 ± 0.01	0.01 ± 0.01	0.02 ± 0.01	0.02 ± 0.01	0.04 ± 0.01	4.25 ± 0.03	0.27 ± 0.01
Ce	0.15 ± 0.01	1.15 ± 0.03	0.02 ± 0.01	0.56 ± 0.04	0.01 ± 0.01	0.09 ± 0.01	0.05 ± 0.05	0.12 ± 0.01	20.08 ± 0.17	0.95 ± 0.01
Nd	0.16 ± 0.01	0.45 ± 0.01	0.02 ± 0.01	0.29 ± 0.01	0.01 ± 0.01	0.22 ± 0.02	0.09 ± 0.01	0.22 ± 0.01	26.40 ± 0.04	1.76 ± 0.01
Sm	0.09 ± 0.01	0.22 ± 0.01	0.03 ± 0.01	0.10 ± 0.01	0.02 ± 0.01	0.18 ± 0.01	0.11 ± 0.01	0.21 ± 0.01	13.53 ± 0.02	1.77 ± 0.01
Eu	0.03 ± 0.01	0.07 ± 0.01	0.01 ± 0.01	0.04 ± 0.01	0.01 ± 0.01	0.05 ± 0.01	0.23 ± 0.01	0.07 ± 0.01	3.12 ± 0.02	0.36 ± 0.01
Dy	0.24 ± 0.01	0.26 ± 0.02	0.01 ± 0.01	0.16 ± 0.01	0.07 ± 0.01	0.93 ± 0.04	0.43 ± 0.02	1.20 ± 0.03	18.89 ± 0.10	9.90 ± 0.05
Er	0.19 ± 0.01	0.18 ± 0.01	0.04 ± 0.01	0.09 ± 0.01	0.05 ± 0.01				10.97 ± 0.07	
Yb	0.19 ± 0.01	0.11 ± 0.01	0.07 ± 0.01	0.06 ± 0.01	0.03 ± 0.01	0.55 ± 0.03	0.32 ± 0.02	0.72 ± 0.02	8.03 ± 0.03	5.95 ± 0.05
$^{147}Sm/^{144}Nd$	0.33 ± 0.02	0.30 ± 0.02	0.84 ± 0.08	0.21 ± 0.01	0.75 ± 0.11	0.51 ± 0.05	0.72 ± 0.06	0.56 ± 0.03	0.31 ± 0.01	0.61 ± 0.01

Major element oxides in wt%. Trace element concentration in ppm. Error reported as standard error.

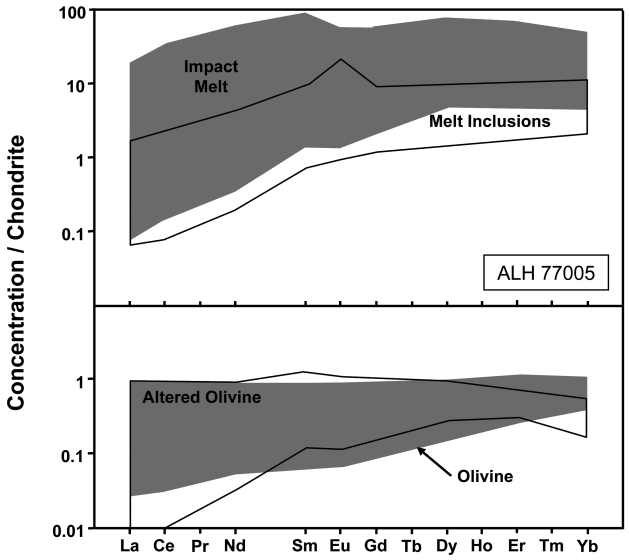

Fig. 4. Rare earth element plot of impact melt, melt inclusions, altered olivine, and olivine from ALH 77005. Note that the altered olivine and olivine contain approximately the same abundances of REEs. Also note the high REE abundances in the impact melt relative to the melt inclusion glass.

is inconsistent with the estimated purity of the DaG 476 maskelynite mineral fraction (>99%) (Borg et al. 2003).

Two observations suggest that the melt inclusion glasses and the high-Si mesostasis are related by igneous crystallization and/or mixing. First, microprobe analyses of 25 different melt inclusions and high-Si mesostasis show a linear trend of decreasing Al_2O_3 abundance (31–0.5 wt%) with increasing SiO_2 abundance (52–90 wt%) (Table 1). Second, the melt inclusions and high-Si mesostasis have similar REE patterns, although the high-Si mesostasis has a slightly more LREE-depleted pattern and, on average, a slightly larger negative Eu anomaly than the melt inclusions (Fig. 2).

Fractional crystallization models were generated in an attempt to reconcile the differences between the melt inclusions and the high-Si mesostasis. Major element data for the melt inclusions and high-Si mesostasis were averaged and normalized to 100% in order to remove any effects of low microprobe totals due to hydration. The majority of the major element data for the high-Si mesostasis could be reproduced with 20–30% crystallization of plagioclase and merrillite from a melt inclusion-composition melt. Likewise, the slopes of the REE patterns of the melt inclusions and the high-Si mesostasis may also be related by 20–30% crystallization of 90% plagioclase and 10% merrillite, provided the Eu partition coefficient for plagioclase is approximately 3. Because Eu partition coefficients for plagioclase in rhyolite can be considerably larger than 3, we consider a value of 3 to be a minimum value (Nash and Crecraft 1985; Bacon and Druitt 1988).

The results of the fractional crystallization models, however, did not explain the high SiO_2 and low Al_2O_3 concentrations in the high-Si mesostasis. Approximately 40% crystallization of a pure Al_2O_3 phase is required to bring the alumina concentration down to match that of the high-Si

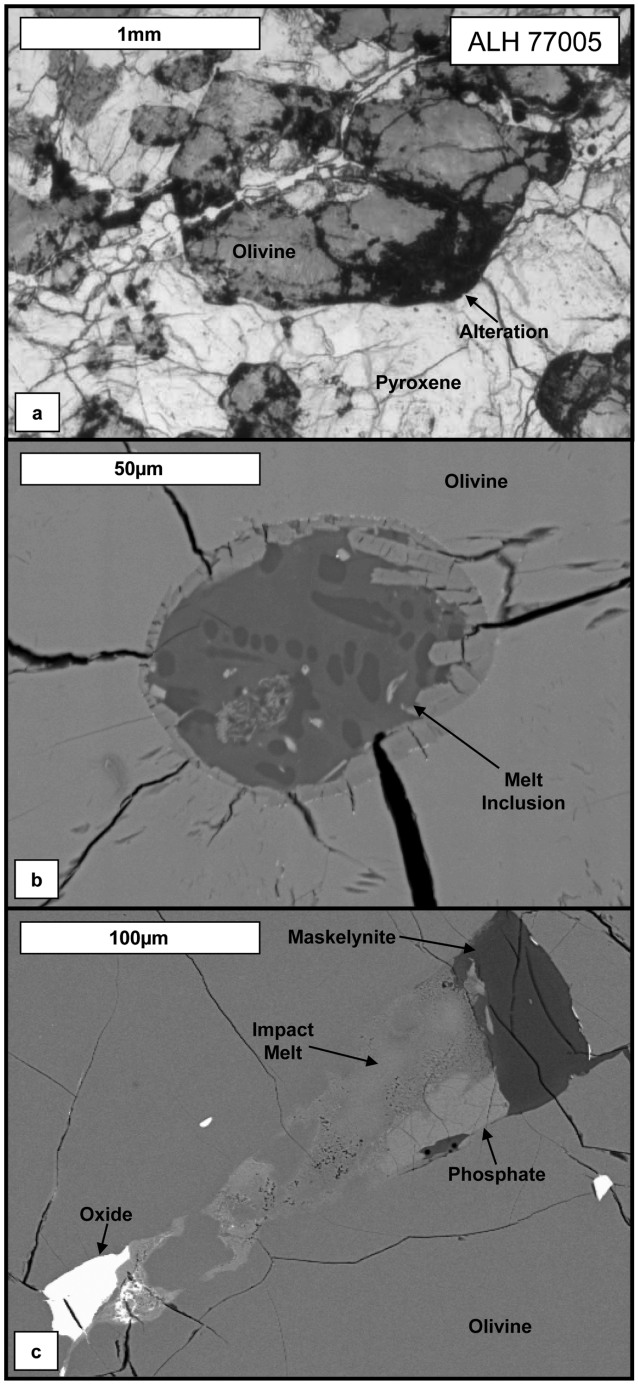

Fig. 5. Photomicrograph and SEM backscatter images of ALH 77005. a) Transmitted light photomicrograph of brown olivines and associated alteration in ALH 77005, 34. b) Backscattered electron image of a melt inclusion. Note the radial fractures similar to those observed in DaG 476, as well as the dark areas within the inclusion indicative of high silica abundances. c) Impact melt glass (30im5) in olivine containing maskelynite, phosphate, and oxide. Note that the impact melt glass is completely enclosed within the olivine.

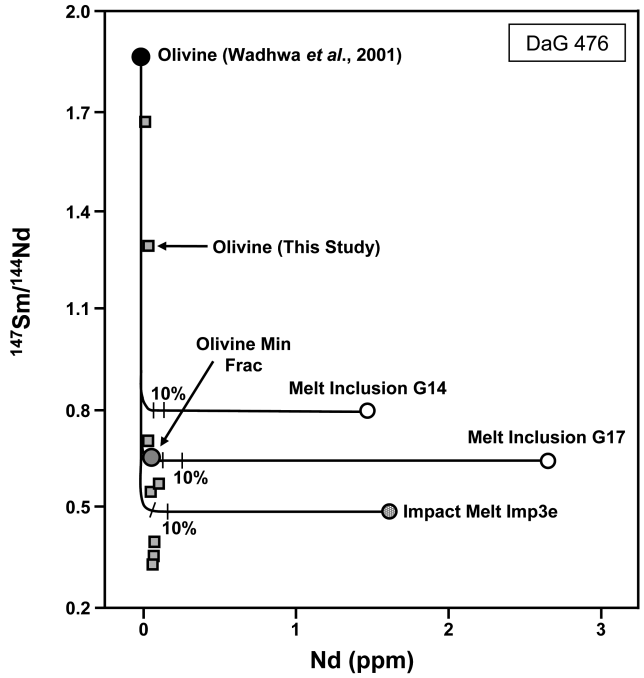

Fig. 6. Mixing models for DaG 476 olivine. Note that the mineral fraction lies on the mixing line between olivine and melt inclusion G17. Approximately 3% of the melt inclusion or 4% of impact melt Imp3e is needed to reproduce the $^{147}Sm/^{144}Nd$ ratio of the olivine mineral fraction. Mineral fraction data from Borg et al. (2003). End-member olivine composition from Wadhwa et al. (2001). Tick marks are at 5% and 10%, respectively.

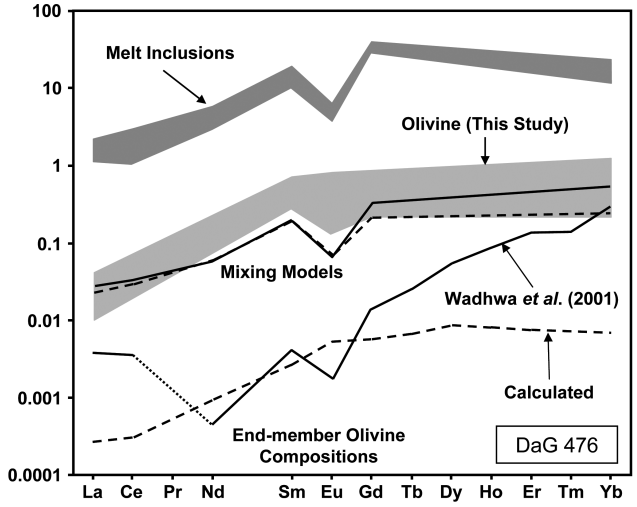

Fig. 7. Mixing models illustrating the influence of the melt inclusions on the REE patterns of olivine in DaG 476. These models demonstrate that the REE patterns observed in the olivines in this study are dominated by the REE abundances of the melt inclusions, and are only slightly influenced by terrestrial alteration. End-member olivine compositions, represented by the lowermost solid and dashed lines, were obtained from Wadhwa et al. (2001) (solid line) and by calculating the average olivine composition in equilibrium with the bulk rock REE pattern of Barrat et al. (2001) using the partition coefficients determined by McKenzie and O'Nions (1991) (dashed line). The uppermost lines are the results of mixing models combining 1% average melt inclusion with olivine composition of Wadhwa et al. (2001) (solid line) and the average olivine composition in equilibrium with the bulk rock (dashed line).

mesostasis. Furthermore, these fractional crystallization models do not reproduce the low REE abundances observed in the high-Si mesostasis. The low REE and K abundances of the high-Si mesostasis preclude its formation by either alteration of a rhyolitic glass or by liquid immiscibility from a less evolved melt (Shearer et al. 2001). Instead, the low REE abundances of the high-Si mesostasis in DaG 476 may be reconciled with the addition of a component that does not contain REEs—in essence a dilution effect. Because of the high silica concentration in the mesostasis, a pure silica component seems likely.

The addition of pure silica to the mesostasis may be plausible given that: 1) many of the melt inclusions in olivine have a rhyolitic composition and are therefore capable of crystallizing quartz, 2) coesite has been observed in melt inclusions from ALH 77005 (Jagoutz 1989), and 3) silica addition would account for the high SiO_2 concentration measured in the mesostasis. In fact, the high silica abundance of the high-Si mesostasis can be reconciled if the mesostasis was contaminated by the addition of approximately 90% pure silica. Thus, the melt inclusions and the high-Si mesostasis, and the various high-Si mesostasis compositions, can be related by differing amounts of crystallization of plagioclase and merrillite, and differing amounts of silica addition during shock melting.

The composition of the undiluted mesostasis present in the maskelynite mineral fraction is calculated from the high-Si mesostasis compositions (Table 1) after 90% silica has been removed. Consequently, this composition has approximately 10 times higher abundances of REEs than the high-Si mesostasis. Mixing models demonstrate that approximately 3% of this mesostasis component is necessary to account for the $^{147}Sm/^{144}Nd$ ratio of the maskelynite mineral fraction (Fig. 8). This lower proportion of contaminant in the mineral fractions is more consistent with their estimated purity.

Mixing Models for Allan Hills 77005 Olivine Compositions

The ALH 77005 olivine mineral fractions lie below the Sm-Nd isochron and have abnormally low $^{147}Sm/^{144}Nd$ ratios. The position of the olivine mineral fractions on the Sm-Nd diagram could be the result of the presence of alteration products or the addition of impact melt containing extraneous material that is not in equilibrium with the rock. These possibilities, as well as the role of melt inclusions, are examined below.

Alteration similar to that observed in the olivine is unlikely to influence the Sm-Nd isotopic systematics of the

Table 4. Partition coefficients used in DaG 476 models.

Element	Olivine[a]	Plagioclase[b]	Phosphate[b]
La	0.0004	0.041	26
Ce	0.0005	0.036	26
Nd	0.0010	0.027	26
Sm	0.0013	0.021	26
Eu	0.0016	3.000[c]	23
Dy	0.0017	0.010	22
Er	0.0015	0.009	15
Yb	0.0015	0.005	8

[a]Partition coefficients from McKenzie and O'Nions (1991).
[b]Partition coefficients from Lundberg et al. (1990) after experiments by G. McKay.
[c]Previous value 0.35, adjustment made to reflect the rhyolitic components in the melt inclusions and high-Si mesostasis.

olivine mineral fractions in ALH 77005 because the altered olivine has REE abundances and patterns that are very similar to the unaltered olivine (Fig. 4). Furthermore, indices of alteration, such as SO_3 abundances, do not correlate with REE abundances or patterns, suggesting that alteration has had a minimal effect on the REE systematics of the olivine. Finally, examples of altered olivine are rare in thin section and may not comprise a significant proportion of the meteorite or the hand-picked mineral fractions.

The mixing models presented in Fig. 10 were constructed to determine if the presence of impact melt could account for the relatively low $^{147}Sm/^{144}Nd$ ratios of the ALH 77005 olivine mineral fractions. The olivine with the highest calculated $^{147}Sm/^{144}Nd$ ratio from this study is used as an end-member because it most accurately describes igneous partitioning in this system. Note that the melt inclusions do not have high enough REE abundances or low enough $^{147}Sm/^{144}Nd$ ratios to account for the low $^{147}Sm/^{144}Nd$ ratios of the olivine mineral fractions (Figs. 1b and 10). Figure 10, however, demonstrates that the $^{147}Sm/^{144}Nd$ ratio of the olivine mineral fractions can be nearly reproduced with the addition of less than 1% of impact melt with a composition similar to that of 30im5b. Furthermore, less than 2% of impact melt is required to account for the REE composition of the olivines analyzed in this study. Although the addition of impact melt can reproduce most of the Sm-Nd systematics observed in the olivines, there are some compositions with lower $^{147}Sm/^{144}Nd$ ratios than the most LREE-enriched impact melt. This suggests that a more LREE-enriched impact melt was added to these olivines. Figure 10 models this scenario by using the LREE-enriched bulk rock composition of the Martian meteorite Zagami (Borg et al., Forthcoming) as a proxy for a more LREE-enriched impact melt. Note that the composition of the olivine mineral fractions of Borg et al. (2002) and all of the olivines analyzed in this study can be explained by the inclusion of less than 8% of a component with a Zagami-like Sm-Nd isotopic composition. The olivines analyzed by Lundberg et al. (1990) are still too LREE-enriched to be explained by this mixing model, and may have

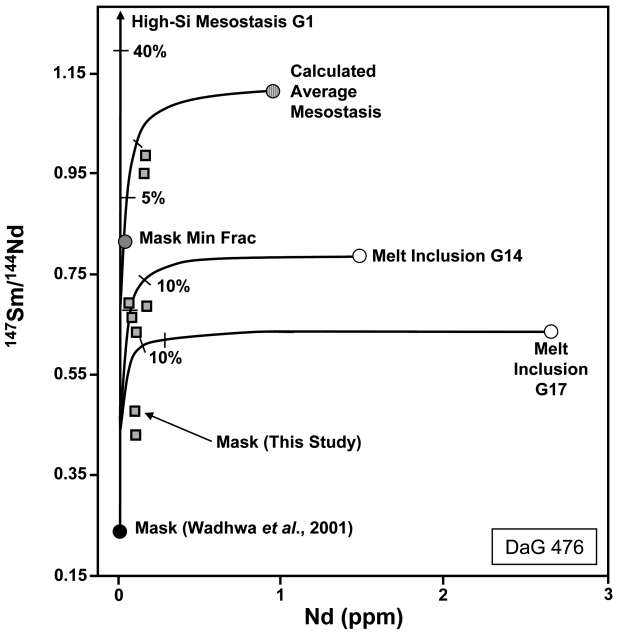

Fig. 8. Mixing models for Dar al Gani 476 maskelynite. Note that the mineral fraction lies along the line between the maskelynite analyzed by Wadhwa et al. (2001) and the composition of the high-Si mesostasis. Also note that the melt inclusions analyzed do not have a high enough $^{147}Sm/^{144}Nd$ ratio to reproduce the isotopic systematics of the mineral fraction. In order to reproduce the Sm-Nd systematics of the maskelynite mineral fraction, a mixture of 20% high-Si mesostasis and 80% maskelynite is required. This result conflicts with the visual estimate of purity of the mineral fractions made by Borg et al. (2003). If the high-Si mesostasis is indeed a combination of a pure silica phase and mesostasis, then the mesostasis must have higher abundances of REEs. The calculated average mesostasis point represents the composition of mesostasis without the high-Si component. The model reveals that inclusion of approximately 3% mesostasis is necessary to account for the isotopic composition of the maskelynite mineral fraction.

compositions that reflect mixing with an even more LREE-enriched component that we have not yet observed.

Mixing of olivine with the impact melt observed in this study is consistent with the major element compositions of the olivine. Because the major element composition of the impact melt is roughly similar to that of the olivine, the only noticeable effect of inclusion of impact melt in the olivine is the increase of elements that do not typically reside in the olivine structure relative to the other olivines observed in ALH 77005. For example, some of the olivine compositions show significant enrichments (up to 0.7 wt%) of Al_2O_3, Cr_2O_3, and P_2O_5, consistent with the presence of chromium spinels and impact melt. The involvement of impact melt in the olivine is also supported by the observation that the abundances of Al_2O_3, Cr_2O_3, and P_2O_5 decrease with distance from the impact melt, suggesting that the contaminant was added from the exterior of the olivine.

The impact melts are the only material analyzed during this study that have high enough Nd abundances and low

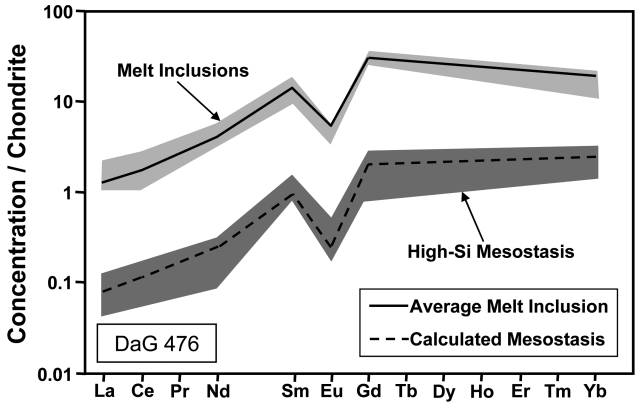

Fig. 9. An REE diagram illustrating the results of trace element modeling to establish a relationship between the melt inclusions and the high-Si mesostasis in DaG 476. The black line denotes the average melt inclusion composition used in the trace element model. The dashed line shows the calculated composition after 20–30% crystallization of 90% plagioclase and 10% merrillite, followed by a dilution of the rare earth elements by addition of a pure silica component. Partition coefficients used in this model are listed in Table 4.

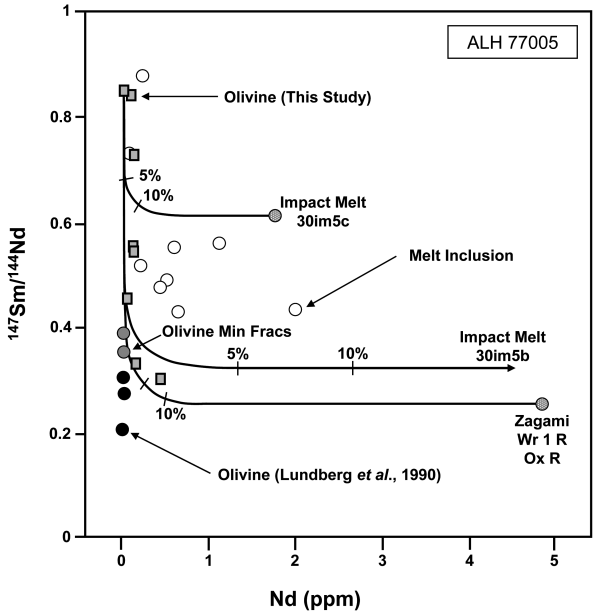

Fig. 10. Mixing models of melt inclusions, impact melt, and olivine from ALH 77005. The data indicate that less than 1% of impact melt with a composition similar to 30im5b is necessary to reproduce the composition of the olivine mineral fractions of Borg et al. (2002), as well as the majority of the olivines in this study. Alternatively, a 3% inclusion of an impact melt with a Zagami-like composition in the olivines could explain the $^{147}Sm/^{144}Nd$ ratios of the olivine mineral fractions. The olivine data from Lundberg et al. (1990) may be the result of mixing olivine with an impact melt more LREE-enriched than the impact melts measured in this study. Note that the melt inclusions do not have sufficiently low $^{147}Sm/^{144}Nd$ to shift the composition of the olivine mineral fractions in the appropriate manner.

enough $^{147}Sm/^{144}Nd$ ratios to approach the compositions of the olivine mineral fraction compositions as well as the olivine compositions obtained by SIMS. It therefore seems likely that the presence of impact melts in the olivine mineral fractions is responsible for their low $^{147}Sm/^{144}Nd$ ratios. However, to account for the low $^{143}Nd/^{144}Nd$ ratios of the olivine mineral fractions, the impact melt must contain an extraneous component characterized by an unradiogenic Nd isotopic signature. Rao et al. (1999) noted that impact melts from Elephant Moraine (EET) 79001 contain a Martian soil component that is not expected to be in isotopic equilibrium with the bulk rock. Addition of a similar component in the impact melt from ALH 77005 could account for the Sm-Nd isotopic systematics of the olivine mineral fractions. In fact, when the Sm-Nd isotopic systematics of ALH 77005 and Zagami are compared, the olivine mineral fractions in ALH 77005 lie along a mixing line with the Zagami whole rock. The end-point of this mixing line, where it intercepts the ALH 77005 isochron, is $^{147}Sm/^{144}Nd \approx 0.6$ and lies between the ALH 77005 pyroxene mineral fractions (not shown). The pyroxene and maskelynite mineral fractions are unlikely to be affected by the small addition of impact melt because they have higher REE abundances and would therefore require larger amounts of impact melt to influence their positions on the isochron. Furthermore, impurities in the pyroxene and maskelynite mineral fractions are easier to separate during hand-picking because the color differences between pyroxene, maskelynite, and the impact melt are greater. Thus, the ALH 77005 Sm-Nd isochron of Borg et al. (2002), defined by pyroxene, maskelynite, whole rock, and leachate fractions, is robust.

Although small additions of impact melt may influence the $^{147}Sm/^{144}Nd$ ratios of the ALH 77005 olivine mineral fractions, the impact melt does not appear to have influenced the Rb/Sr isotopic ratio of the olivine mineral fractions. The fact that the Rb-Sr isotopic systematics are not disturbed implies that the extraneous component added to the olivine impact melt has a Sr/Nd ratio substantially less than the Sr/Nd ratio of 109 for the olivine itself (Borg et al. 2002). Note that the Sr/Nd ratios of non-cumulate bulk Martian meteorites vary from 9 to 44 (Warren and Kallemeyn 1997; Dreibus et al. 2002), with Zagami at 12 (Borg et al., Forthcoming), and could satisfy the Rb-Sr and Sm-Nd isotopic criteria required of the contaminant.

Fine-Scale Redistribution of Elements

Our models suggest that the olivine and maskelynite mineral fractions from DaG 476 have Sm-Nd isotopic systematics that reflect the presence of melt inclusions and mesostasis, respectively. In contrast, the isotopic compositions of the ALH 77005 olivine mineral fractions appear to be controlled by the presence of impact melt containing a non-indigenous component. However, in situ olivine and maskelynite analyses from both meteorites often have Sm and Nd abundances that are very similar to those of

the mineral fractions. This suggest that the melt inclusions, mesostasis, and impact melt are incorporated into the olivine and maskelynite on a fine (<30 μm) scale.

Because a limited amount of mesostasis is required to leverage the maskelynite compositions and because compositional zonations that could be attributed to diffusion are not readily apparent, it appears that the maskelynite has become enriched in mesostasis by a physical mixing process. This is supported by evidence that plagioclase in Martian meteorites can melt and flow (e.g., Ikeda 1994; Chen and El Goresy 2000; Malavergne et al. 2001), thus facilitating mixing. Evidence for the melting and flowing of maskelynite in DaG 476 includes the absence of shock-induced fractures in maskelynite as well as the observed flow lines of melted pyroxene and mesostasis in the maskelynite (Chen and El Goresy 2000). Similarly, evidence for melting and flowing of maskelynite in ALH 77005 includes the presence of vesicles and schlieren of melted olivine and pyroxene in the maskelynite (Treiman et al. 1994; Treiman and Treado 1998).

Accounting for the anomalous presence of Al_2O_3, Cr_2O_3, P_2O_5, and REEs in some olivines on a fine scale is more difficult. Three potential mechanisms that could account for the relatively high abundances of these elements derived from melt inclusions and impact melt in some olivines include: 1) diffusion associated with shock heating, 2) incorporation of incompatible elements into defect sites produced by shock (Adadurov et al. 1971), and 3) quench cooling of olivine-melt mixtures (Treiman et al. 1994). Diffusion of highly incompatible elements, such as Al, Cr, P, and REE into the olivine structure at the elevated abundances observed here is unlikely. It therefore seems that the distribution of these elements into the olivine must be associated with structural changes in the olivine resulting from shock processes.

The presence of Fe^{3+} in olivine in ALH 77005 illustrates one of the changes that can occur during shock and implies a mobilization of oxygen within the olivine crystal (Bauer 1979; Ostertag et al. 1984; Puga et al. 1998). Mobilization of oxygen during shock may produce defects in minerals and allow mobilized elements from other phases to be incorporated into the minerals along those defect structures. In fact, Boslough (1991) noted that shock produces a higher density of defects in shocked minerals relative to their unshocked counterparts. These shocked materials have been shown to accept larger, typically incompatible, ions into their structure (Adadurov et al. 1971). Although this mechanism cannot account for the incorporation of impact melt into the olivines, as required by the mixing models for ALH 77005, it may account for the REE systematics of the DaG 476 olivines analyzed in this study. Thus, the high abundances of REE derived from melt inclusions may be incorporated into defects in the host olivine as a result of shock processes.

Addition of impact melts to the olivine is more complicated because it requires addition of a component that is extraneous to the olivine. Treiman et al. (1994) studied the structure of olivine within 1 mm of an impact melt in LEW 88516. The olivines in this lherzolitic shergottite demonstrate a progressive change in crystal structure from zones of deformation to zones of recrystallization to zones of partial melting with decreasing distance to the impact melt. It is therefore probable that the olivines in ALH 77005 have heterogeneous compositions that reflect the addition of an extraneous component such as impact melt. This hypothesis is supported by the spatial correlation between impact melt and the increased abundances of Al_2O_3, Cr_2O_3, and P_2O_5 in some of the olivines in ALH 77005. It is therefore possible that some of the olivine was partially melted, mixed with impact melt, and quenched before highly incompatible elements could be removed or isolated into discrete phases.

CONCLUSION

The positions of the olivine and maskelynite mineral fractions on the DaG 476 Sm-Nd isochron, as well as the olivine mineral fractions lying off the ALH 77005 Sm-Nd isochron, indicate fundamental disturbances in the isotopic signatures of these mineral fractions. Thermal ionization mass spectrometry and SIMS analyses both show that maskelynite in DaG 476 is LREE-depleted relative to chondrite and that the REE patterns of most olivines in both DaG 476 and ALH 77005 are not LREE-depleted enough to be indicative of igneous partitioning. In addition, the olivine mineral fractions from ALH 77005 contain an unradiogenic Nd component that is not in isotopic equilibrium with the rock. Mixing models demonstrate that olivine and maskelynite in DaG 476 are shifted to relatively low and high $^{147}Sm/^{144}Nd$ ratios, respectively, by the addition of melt inclusions and mesostasis. Crystallization models demonstrate that the melt inclusions and mesostasis are related by varying degrees of plagioclase and phosphate crystallization and the addition of a high SiO_2 component. Since the materials that are included in the olivine and maskelynite mineral fractions are igneous, the isochron of Borg et al. (2003) represents the age of DaG 476. Olivine in ALH 77005 appears to be shifted to low $^{147}Sm/^{144}Nd$ ratios, and off the Sm-Nd isochron, by the addition of impact melt possibly containing a surficial component with a Zagami-like Sm-Nd isotopic composition. The fact that the remaining fractions define an isochron that is concordant with the Rb-Sr age for ALH 77005 (Borg et al. 2002) indicates that the Sm-Nd isochron is robust despite the addition of this component. Contamination resulting in LREE enrichment of olivines in both DaG 476 and ALH 77005, and relative LREE depletion of maskelynite in DaG 476, occurs on a fine (<30 μm) scale. This fine-scale REE distribution suggests that the contaminants are added to the mineral fractions as a result of shock processes. Ultimately, this study demonstrates that, despite disturbances to the Sm-Nd isotopic systematics, the age of meteorites can be gleaned from pure mineral separates and an understanding of the mechanisms that disturb their isotopic systems.

Acknowledgments–This research was funded by NASA grant NAG5-11555 to L. E. Borg, NASA grant MRA 97-282 to J. J. Papike, and the Institute of Meteoritics. We appreciate the use of thin sections of ALH 77005 from NASA Johnson Space Center, Houston, Texas, USA, and DaG 476 from the Institut für Chemie in Mainz, Germany. Technical support was provided by Mike Spilde, Jim Karner, and Justin Hagerty. Kimberly Davidson aided in sample preparation. Cyrena Goodrich, John Longhi, Larry Nyquist, and Jon Patchett provided constructive reviews, which improved this paper.

Editorial Handling—Dr. Cyrena Goodrich

REFERENCES

Adadurov G. A., Breusov O. N., Dremin A. N., and Drobyshev, V. N. 1971. The capacity of neodymium oxide for hydration after treatment with high-pressure pulses. *Russian Journal of Inorganic Chemistry* 16:1073–1074.

Anders E., and Grevesse N. 1989. Abundances of the elements—Meteoritic and solar. *Geochimica et Cosmochimica Acta* 53:197–214.

Bacon C. R. and Druitt T. H. 1988. Compositional evolution of the zoned calcalkaline magma chamber of Mt. Mazama, Crater Lake, Oregon. *Contributions to Mineralogy and Petrology* 98:224–256.

Barrat J. A., Blichert-Toft J., Nesbitt R. W., and Keller F. 2001. Bulk chemistry of the Saharan shergottite Dar al Gani 476. *Meteoritics & Planetary Science* 36: 23–29.

Bauer J. F. 1979. Experimental shock metamorphism of mono- and polycrystalline olivine: A comparative study. 10th Lunar and Planetary Science Conference. pp. 2573–2596.

Boettcher A. L. 1984. The system SiO_2-H_2O-CO_2: Melting, solubility mechanisms of carbon, and liquid structure to high pressures. *American Mineralogist* 69:823–833.

Borg L. E., Nyquist L. E., Wiesmann H., and Reese Y. 2002. Constraints on the petrogenesis of Martian meteorites from the Rb-Sr and Sm-Nd isotopic systematics of the lherzolitic shergottites ALH 77005 and LEW 88516. *Geochimica et Cosmochimica Acta* 66:2037–2053.

Borg L. E., Nyquist L. E., Wiesmann H., Shih C.-Y., and Reese Y. 2003. The age of Dar al Gani 476 and the differentiation history of the Martian meteorites inferred from their radiogenic isotopic systematics. *Geochimica et Cosmochimica Acta* 67:3519–3536.

Borg L. E., Edmunson J., and Asmerom Y. Forthcoming. Constraints on the U-Pb isotopic systematics of Mars inferred from a combined U-Pb, Rb-Sr, and Sm-Nd isotopic study of the Martian meteorite Zagami. *Geochimica et Cosmochimica Acta*.

Boslough M. B. 1991. Shock modification and chemistry and planetary geologic processes. *Annual Reviews in Earth and Planetary Science* 19:101–130.

Champness P. E. 1970. Nucleation and growth of iron oxides in olivines, $(Mg,Fe)_2SiO_4$. *Mineralogical Magazine* 37:790–800.

Chen M. and El Goresy A. 2000. The nature of maskelynite in shocked meteorites: Not diaplectic glass but a glass quenched from shock-induced dense melt at high pressures. *Earth and Planetary Science Letters* 179:489–502.

Crozaz G., and Wadhwa M. 2001. The terrestial alteration of Saharan shergottites Dar al Gani 476 and 489: A case study of weathering in a hot desert environment. *Geochimica et Cosmochimica Acta* 65:971–978.

Crozaz G., Floss C., and Wadhwa M. 2003. Chemical alteration and REE mobilization in meteorites from hot and cold deserts. *Geochimica et Cosmochimica Acta* 67:4727–4741.

Dreibus G., Wlotzka F., Huisl W., Jagoutz E., Kubny A., and Spettel B. 2002. Chemistry and petrology of the most feldspathic shergottite: Dhofar 387 (abstract). *Meteoritics & Planetary Science* 37:A43.

Folco L., Franchi I. A., D'Orazio M., Rocchi S., and Schultz L. 2000. A new Martian meteorite from the Sahara: The shergottite Dar al Gani 489. *Meteoritics & Planetary Science* 35:827–839.

Goodrich C. A. 2002. Olivine-phyric Martian basalts: A new type of shergottite. *Meteoritics & Planetary Science* 37:B31–B34.

Haggerty S. E., and Baker I. 1967. The alteration of olivine in basaltic and associated lavas, part 1: High temperature alteration. *Contributions to Mineralogy and Petrology* 16:233–257.

Harvey R. P., Wadhwa M., McSween H. Y., Jr., and Crozaz G. 1993. Petrology, mineral chemistry, and petrogenesis of Antarctic shergottite LEW 88516. *Geochimica et Cosmochimica Acta* 57: 4769–4783.

Ikeda Y. 1994. Petrography and petrology of the ALH A77005 shergottite. *Proceedings of the NIPR Symposium on Antarctic Meteorites* 7:9–29.

Jagoutz E. 1989. Sr and Nd isotopic systematics in ALH A77005: Age of shock metamorphism in shergottites and magmatic differentiation on Mars. *Geochimica et Cosmochimica Acta* 53: 2429–2441.

Lee M. R. and Bland P. A. 2004. Mechanisms of weathering of meteorites recovered from hot and cold deserts and the formation of phyllosilicates. *Geochimica et Cosmochimica Acta* 68:893–916.

Longhi J. and Pan V. 1989. The parent magmas of the SNC meteorites (abstract). 19th Lunar and Planetary Science Conference. pp. 451–464.

Lundberg L. L., Crozaz G., and McSween H. Y., Jr. 1990. Rare earth elements in minerals of the ALH A77005 shergottite and implications for its parent magma and crystallization history. *Geochimica et Cosmochimica Acta* 54:2535–2547.

Malavergne V., Guyot F., Benzerara K., and Martinez I. 2001. Description of new shock-induced phases in the Shergotty, Zagami, Nakhla, and Chassigny meteorites. *Meteoritics & Planetary Science* 36:1297–1305.

McKenzie D. and O'Nions R. K. 1991. Partial melt distributions from inversion of rare earth element concentrations. *Journal of Petrology* 32:1021–1091.

McSween H. Y., Jr., Taylor L. A., and Stolper E. M. 1979. Allan Hills 77005: A new meteorite type found in Antarctica. *Science* 204: 1201–1203.

Mikouchi T. 1999. Preliminary examination of Dar al Gani 476: A new basaltic Martian meteorite similar to lithology A of EET A79001 (abstract #1557). 30th Lunar and Planetary Science Conference. CD-ROM.

Mysen B. O., Eggler D. H., Seitz M. G., and Holloway J. R. 1976. Carbon dioxide in silicate melts and crystals. Part I. Solubility measurements. *American Journal of Science* 276:455–479.

Nash W. P., and Crecraft H. R. 1985. Partition coefficients for trace elements in silicic magmas. *Geochimica et Cosmochimica Acta* 49:2309–2322.

Nyquist L. E., Wooden J., Bansal B., Wiesmann H., McKay G., and Bogard D. D. 1979. Rb-Sr age of the Shergotty achondrite and implications for metamorphic resetting of isochron ages. *Geochimica et Cosmochimica Acta* 43:1057–1074.

Ostertag R., Amthauer G., Rager H., and McSween H. Y., Jr. 1984. Fe^{3+} in shocked olivine crystals of the ALH A77005 meteorite. *Earth and Planetary Science Letters* 67:162–166.

Pan V., Holloway J. R., and Hervig R. L. 1991. The pressure and temperature dependence of carbon dioxide solubility in

tholeiitic basalt melts. *Geochimica et Cosmochimica Acta* 55: 1587–1595.

Puga E., Jagoutz E., Nieto J. M., Diaz de Federico A., and Ruiz-Cruz M. D. 1998. On the origin of the brown color in ALH A77005 olivine (abstract #1375). 29th Lunar and Planetary Science Conference. CD-ROM.

Putnis A. 1979. Electron petrography of high-temperature oxidation in olivine from the Rhum Layered Intrusion. *Mineralogical Magazine* 43:293–296.

Rao M. N., Borg L. E., McKay D. S., and Wentworth S. J. 1999. Martian soil component in impact glasses in a Martian meteorite. *Geophysical Research Letters* 26:3265–3268.

Shearer C. K., Papike J. J., and Spilde M. N. 2001. Trace-element partitioning between immiscible lunar melts: An example from naturally occurring lunar melt inclusions. *American Mineralogist* 86:238–246.

Shih C.-Y., Nyquist L. E., Bogard D. D., McKay G. A., Wooden J. L., Bansal B. M., and Wiesmann H. 1982. Chronology and petrogenesis of young achondrites, Shergotty, Zagami, and ALH A77005: Late magmatism on a geologically active planet. *Geochimica et Cosmochimica Acta* 46:2323–2344.

Smith M. R., Laul J. C., Ma M.-S., Huston T., Verkouteren R. M., Lipschutz M. E., and Schmitt R. A. 1984. Petrogenesis of the SNC (shergottites, nakhlites, chassignites) meteorites—Implications for their origin from a large, dynamic planet, possibly Mars. *Journal of Geophysical Research* 89:B612–B630.

Snyder G. A., Taylor L. A., and Neal C. R. 1992. A chemical model for generating the sources of mare basalts: Combined equilibrium and fractional crystallization of the lunar magmasphere. *Geochimica et Cosmochimica Acta* 56:3809–3823.

Treiman A. and Treado P. 1998. Martian maskelynite? Raman spectra of plagioclase-composition glasses from ALH 84001, EET A79001, and ALH A77005 (abstract #1196). 29th Lunar and Planetary Science Conference. CD-ROM.

Treiman A. H., McKay G. A., Bogard D. D., Wang M.-S., Lipschutz M. E., Mittlefehldt D. W., Keller L., Lindstrom M. M., and Garrison D. 1994. Comparison of the LEW 88516 and ALH 77005 Martian meteorites: Similar but distinct. *Meteoritics* 29: 581–592.

Wadhwa M., Lentz R. C. F., McSween H. Y., Jr., and Crozaz G. 2001. A petrologic and trace element study of Dar al Gani 476 and Dar al Gani 489: Twin meteorites with affinities to basaltic and lherzolitic shergottites. *Meteoritics & Planetary Science* 36:195–208.

Warren P. H. and Kallemeyn G. W. 1997. Yamato-793605, EET 79001, and other presumed Martian meteorites: Compositional clues to their origins. *Antarctic Meteteorite Research* 10:61–81.

Warren P., Kallemeyn G. W., and Kyte F. T. 1999. Origin of planetary cores: Evidence from highly siderophile elements in Martian meteorites. *Geochimica et Cosmochimica Acta* 63:2105–2122.

Zipfel J. and Goodrich C. A. 2001a. Rare earth element systematics of trapped melt inclusions and groundmass phases in Sayh al Uhaymir 005 (abstract #1292). 32nd Lunar and Planetary Science Conference. CD-ROM.

Zipfel J. and Goodrich C. A. 2001b. REE in melt inclusions in olivine of ALH A77005 (abstract). *Meteoritics & Planetary Science* 36: A232–A233.

Zipfel J., Scherer P., Spettel B., Dreibus G., and Schultz L. 2000. Petrology and chemistry of the new shergottite Dar al Gani 476. *Meteoritics & Planetary Science* 35:95–106.